EFFICIENT CLASSIFICATION OF LOW-RESOLUTION RANGE PROFILES OF AUTOMOBILES USING A COMBINATION OF USEFUL FEATURES

Joo-Ho Jung[1] and Sang-Hong Park[2, *]

[1]Department of Electrical Engineering, Pohang University of Science and Technology, Pohang, Gyungbuk, Korea

[2]Department of Electronic Engineering, Pukyong National University, Busan, Korea

Abstract—The range profile (RP) of an automobile is derived by compressing the wideband radar signal, and it can be utilized for the classification and thus contribute to lane change and collision avoidance. However, the limited radar bandwidth due to the cost and the system complexity impedes the successful classification. This paper proposes an efficient method to construct an efficient feature vector of the automobile RP through combined use of the central moment, the information on the maximum-minimum and the peak information. Simulation results using the five automobile models composed of point scatterers and a simple nearest neighbor classifier prove that the proposed method improves the classification result, especially in the multi-aspect classification.

1. INTRODUCTION

Research on radar has been very active in the last few years; much progress has been made, especially for the pre-crush warning radar at 24/26 GHz and the cruise-control radar at 77 GHz bands [1]. Among several radar signatures, the range profile (RP) shows the unique one dimensional distribution of the radar cross-section [2–9] of the automobile and can be effectively used for classification of automobiles which can contribute to anti-collision, lane-change, and automobile control regardless of weather and day-night conditions [10]. RP can also provide two-dimensional radar image of automobiles if the

synthetic aperture radar (SAR) [11–18], the inverse SAR [19] and the jet engine modulation [20] techniques are applied.

However, classification must be automated for this profile to be useful. Moreover, the bandwidth of the radar is limited due to the cost, system complexity and regulations. This impedes successful classification of RPs because of reduced resolution of compressed signal. Hence, it is needed to develop efficient features and classifiers that can discriminate automobiles under low-resolution condition. To date, most researches have focused on the development of the classifier [21, 22]. However, high classification ratios can be achieved by using a simple classifier once the features of each automobile are properly separated in the feature space [23–25].

The central moment (CM) invariant to translation of RPs is a very efficient method that has been recently developed [22]. Compared with conventional methods such as the matching score [26] and the Fourier transform [27] methods, CM is computationally more efficient and robust to the dominant peak of RP especially in classifying high-resolution RPs. This method regards the RP as a probability distribution function (PDF) and utilizes CMs as elements of feature vectors. However, the problem of this method is that high order CMs are sensitive to the variation of RPs since small disturbance of RP caused by the clutter may cause wider fluctuation of high order CMs. The extended high order CM [28] proposed to overcome this fluctuation does not fully improve the performance.

This paper proposes an efficient method of improving the classification performance of low-resolution automobile RPs which uses the feature vector constructed by combining CM and two forms of useful features called maxima-minima information (MMI) and peak information (PI). In simulations that use five automobiles composed of point scatterers and a simple nearest neighbor classifier (NNC), the proposed method is found to significantly improve the classification ratios, especially in multi-aspect classification.

2. SIGNAL MODEL AND PROPOSED METHOD

2.1. Signal Model

For the radar signal, we assume the monostatic chirp waveform

$$r(t) = A_0 e^{j2\pi\left(f_0 t + \frac{B}{2\tau}t^2\right)} \times \text{rect}\left[\frac{t}{\tau}\right], \qquad (1)$$

where $r(t)$ is a transmitted signal at time t, A_0 its amplitude, f_0 the start frequency, B the bandwidth, τ the pulse duration, and rect a function whose value is 1 for $t - \tau/2 \leq t \leq t + \tau/2$ and 0 otherwise.

The received signal reflected from a target composed of K scattering centers is

$$g(t) = \sum_{k=1}^{K} A_k e^{j2\pi[f_0(t-d_k) + \frac{B}{2\tau}(t-d_k)^2]} \times \text{rect}\left[\frac{t - d_k}{\tau}\right], \quad (2)$$

where A_k is the amplitude of scattering center k and d_k the time delay between the radar and scattering center k; d_k is calculated using plane wave approximation, in which the distance to a scattering center is that projected onto the radar line-of-sight vector.

The received signal $g(t)$ is compressed by the matched-filter which is implemented by a correlation between the stored replica $s_r(t)$ and $g(t)$ as follows [29]:

$$s_{out}(t) = \int_{-\infty}^{\infty} s_r(t)g^*(u - t)du. \quad (3)$$

If we define the filter kernel by $h(t) = g^*(-t)$, $s_{out}(t)$ is derived by the following convolution filter,

$$s_{out}(t) = s_r(t) \otimes h(t) = \int_{-\infty}^{\infty} s_u(t)h(t - u)du. \quad (4)$$

Using the convolution-multiplication relationship between the time and the frequency domains, (4) can be implemented in the frequency domain as follows:

$$S_{out}(f) = S_r(f)H_r(f), \quad (5)$$

where $S_{out}(f)$, $S_r(f)$ and $H(f)$ are the Fourier transform of $s_{out}(t)$, $s_r(t)$ and $h(t)$. The compressed output which is the RP is then given by the sum of the following sinc functions:

$$s_{out}(t) = \sum_{k=1}^{K} A_k \tau \text{sinc}(B(t - d_k)). \quad (6)$$

The 3-dB resolution of the matched filter is $c/2B$ where c is the speed of the light. Therefore, wide bandwidth is needed for high resolution RPs.

2.2. Problem of the Existing Method and Proposed Method

In this paper, we utilize the CM as a part of the feature vector because it has already been proven to be very effective for the classification of targets [29]. The RP normalized by the sum of the total values in the RP is regarded as a PDF, and the statistical characteristic of this PDF is usefully characterized by CMs. Therefore, the feature vector

composed of CMs can be effectively applied to automobile recognition. CM of the order q is given by the following formula:

$$\mu_q = \sum_{n=0}^{N_r-1} (n - \eta_r)^q \left[\frac{\bar{p}(n)}{\sum_{i=0}^{N_r-1} \bar{p}(i)} \right], \quad \eta_r = \sum_{n=0}^{N_r-1} n \left[\frac{\bar{p}(n)}{\sum_{i=0}^{N_r-1} \bar{p}(i)} \right], \quad (7)$$

where $\bar{p}(n)$ is the amplitude of the component n in RP normalized by the maximum value and N_r the number of range bins in RP.

The major problem of CM is that RPs of automobiles fluctuate due to the effect of the road and other nearby automobiles. In this case, high order CMs are not adequate because the difference in $(n - \eta_r)^q$ in (7) between the training and the test data becomes larger as q increases. Furthermore, at narrow bandwidth, i.e., at low resolution, automobiles are represented by a small number of range bins; in this case, the low-order CMs cannot uniquely represent the RP due to the information loss. Thus, additional information is needed to construct the feature vector. In this paper, we propose two forms of additional features that can be used in combination with low-order CMs in constituting the feature vector to classify low-resolution RPs. There can be many of existing features such as histogram and correlation, etc., that can be combined with CM. However, these features are not effective because low-resolution RPs do not have many range bins and thus classification performance can be degraded.

The first form proposed in this paper is MMI of RPs. This paper uses the difference of the location and the amplitude among global maximum (GM), local maxima and minima (LMM) larger than a threshold. We denote GM + LMM by MM. Because the location of MMs and the relative difference of MMs are more robust to the fluctuation of RP than CMs, MMI can provide additional information of automobiles. For example, when the number of MMs $a_m = 4$, we can use additional useful elements amounting to $_4C_3 \times 2 = 12$.

Because the number of range bins in the RP of automobiles is very small at narrow bandwidth, complicated peak detection algorithms [30] are not required. Instead, assuming $\bar{p}(i)_{D1} = \bar{p}(i+1) - \bar{p}(i)$ and $\bar{p}(i)_{D2} = \bar{p}(i+1)_{D1} - \bar{p}(i)_{D1}$, we utilized a simple second derivative test of RP to find LMMs as follows:

a) If $\bar{p}(i+1)_{D1} = 0$ and $\bar{p}(i)_{D2} < 0$, then $\bar{p}(i+2)$ is a local maximum.

b) If $\bar{p}(i+1)_{D1} = 0$ and $\bar{p}(i)_{D2} > 0$, then $\bar{p}(i+2)$ is a local minimum.

To remove the effect of noise and small minor MMs, the detected GM and LMMs are thresholded, and the highest l MMs are selected. Because of the small number of range bins, the second derivative test finds MMs accurately (Fig. 1). The amplitude difference MA_{ij} between
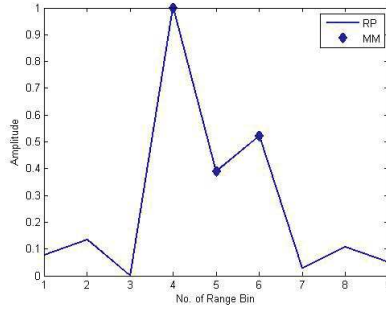
Figure 1. Example of low-resolution RP and MM ($B = 30\,\mathrm{MHz}$, $l = 3$).

MM i and j is defined by

$$MA_{ij} = |\bar{p}(k_i) - \bar{p}(k_j)|, \tag{8}$$

where k_i and k_j are the location of MM i and j. In a similar manner, the location difference MD_{ij} between MM i and j is defined by

$$MD_{ij} = |k_i - k_j|. \tag{9}$$

The second form of feature proposed in this paper is PI. At narrow bandwidth, most of the energy is concentrated around the peak of RP. Therefore, constructing the feature vector using PI can further improve the classification result. Using the location of the peak i_{pe}, we developed the additional elements; the ratio E_p of the peak power and the ratio E_a of the power around the peak with respect to the total power, and the power difference E_i^+ and E_i^- between the peak power and the power at $\pm i$ from the peak, each of which is represented by

$$E_{pe} = \bar{p}(i_{pe})^2, \tag{10}$$

$$E_a = \sum_{m=-a}^{a} \bar{p}(i_{peak} + m)^2, \tag{11}$$

$$E_i^+ = \bar{p}(i_{pe})^2 - \bar{p}(i_{pe} + i)^2, \quad E_i^- = \bar{p}(i_{pe})^2 - \bar{p}(i_{pe} - i)^2. \tag{12}$$

When the proposed combination was used, the length of the feature vector composed of CMs increased from $(p_m - 1)$ to $l_f = (p_m + a_m \times (a_m - 1) + 2n_m + 2)$ as follows:

$$\vec{f} = \left[\vec{C} \vec{M_a} \vec{M_d} \vec{E} \right]^T, \tag{13}$$

where,

$$\vec{C} = [\mu_2 \mu_3 \ldots \mu_{p_m}], \tag{14}$$

$$\vec{M_a} = \left[MA_{12} MA_{13} \ldots MA_{(a_m-1)(a_m)} \right], \tag{15}$$

$$\vec{M}_d = \left[MD_{12} MD_{13} \ldots MD_{(a_m - 1)(a_m)} \right], \tag{16}$$

$$\vec{E} = \left[E_{pe} E_a E_{n_m}^+ E_{n_m - 1}^+ \ldots E_{n_m - 1}^- E_{n_m}^- \right]. \tag{17}$$

p_m is the maximum order of CM, a_m the number of MMs selected, and n_m the number of range bins from the peak. Because of the increased length of the feature vector, automobiles can be better separated in the feature space.

Using the proposed feature vector, the total train data of N_c automobiles and N_a angles are obtained as follows:

$$\mathbf{F} = \begin{bmatrix} f_{11} & f_{12} & \cdots & f_{1,N_c \times N_a} \\ f_{21} & f_{22} & \cdots & f_{2,N_c \times N_a} \\ \vdots & \vdots & \ddots & \vdots \\ f_{l_f,1} & f_{l_f,2} & \cdots & f_{l_f,N_c \times N_a} \end{bmatrix}, \tag{18}$$

where f_{ij} is the ith element of the feature vector j, i.e., $\vec{f}_j$. Because the range of each element in the feature is different, the magnitude of element f_{ij} in (18) must be transformed to have the same weight in the feature space. Thus, we used the following rule to construct the normalized train matrix $\vec{F}$ whose elements are between zero and unity as follows [31]:

$$\bar{f}_{ij} = \frac{f_{ij} - f_{i,\min}}{f_{i,\max} - f_{i,\min}}, \tag{19}$$

where $f_{i,\max}$ and $f_{i,\min}$ are the maximum and minimum in the column of $\mathbf{F}$ in (18).

To reduce the classification time and remove the redundancy, the principal component analysis was applied [31]. This method first derives the sample mean vector $\vec{m}$ and the covariance matrix $\mathbf{R}$ as follows:

$$\vec{m} = \frac{1}{Q} \sum_{k=1}^{Q} \vec{f}_k, \tag{20}$$

$$\mathbf{R} = \frac{1}{Q-1} \sum_{k=1}^{Q} \left(\vec{f}_k - \vec{m} \right) \left(\vec{f}_k - \vec{m} \right)^T, \tag{21}$$

where $\vec{f}$ is the kth column vector of the normalized train matrix $\bar{F}$, $Q = N_c \times N_a$. Then, $l_f \times O$ transformation matrix $\mathbf{W}$ is constructed using the O eigen vectors of R corresponding to highest O eigen values corresponding to highest O eigen values. The $O \times 1$ feature vector transformed by T matrix is as follows:

$$\vec{x} = \mathbf{W}^T \vec{f}. \tag{22}$$

In the test phase, the test feature vector of an unknown target is normalized using (19) and transformed using (22).

In classification, we used a simple NNC which utilizes a simple Euclidean distance between two vectors as follows:

$$d\left(\vec{x}_i, \vec{x}_j\right) = \sqrt{\sum_{k=1}^{O}\left(\vec{x}_i(k) - \vec{x}_j(k)\right)^2}. \qquad (23)$$

Assuming that the test vector of an unknown automobile is $\vec{x}_u$ and that the train vector of the automobile i is $\vec{x}_i$, classification was conducted based on the following rule:

$$i^* = \min_i d\left(\vec{x}_u, \vec{x}_i\right). \qquad (24)$$

In other words, the train automobile whose feature vector yields the shortest Euclidean distance to the test vector is judged to be the one that the unknown automobile belongs to. To further improve the classification result, we applied the multi-aspect classification method using the test vectors derived at several aspects, which is

$$i^* = \max_k N_k, \qquad (25)$$

where N_k denotes the number of kth class decisions made by (22). The overall classification procedure is summarized in Fig. 2.
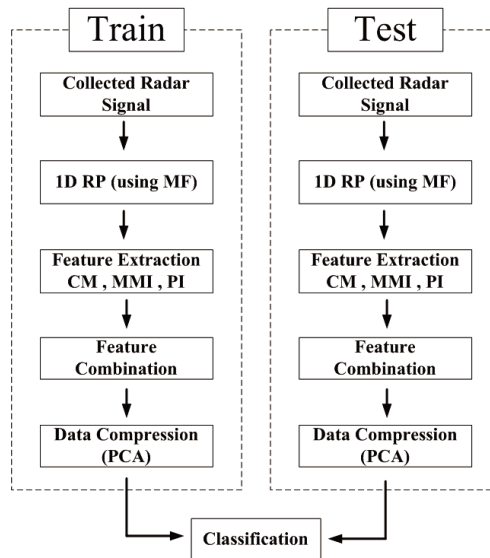

Figure 2. Classification procedure.

3. SIMULATION RESULTS

In simulations, we used five automobiles consisting of isotropic point scatterers (Fig. 3). To be realistic, we modeled the automobiles using the 3D CAD data of the real-sized automobiles: a sedan, a compact car, a bus, a minivan and a truck (www.3dcadbrowser.com). For the radar system, we used a monostatic chirp radar with pulse repetition frequency $= 2\,\text{kHz}$, center frequency $= 24\,\text{GHz}$, bandwidth $= 30\,\text{MHz}$ and pulse width $\tau = 30\,\mu\text{s}$. Targets were represented by a small number

(a) Sedan

(b) Compact car

(c) Bus

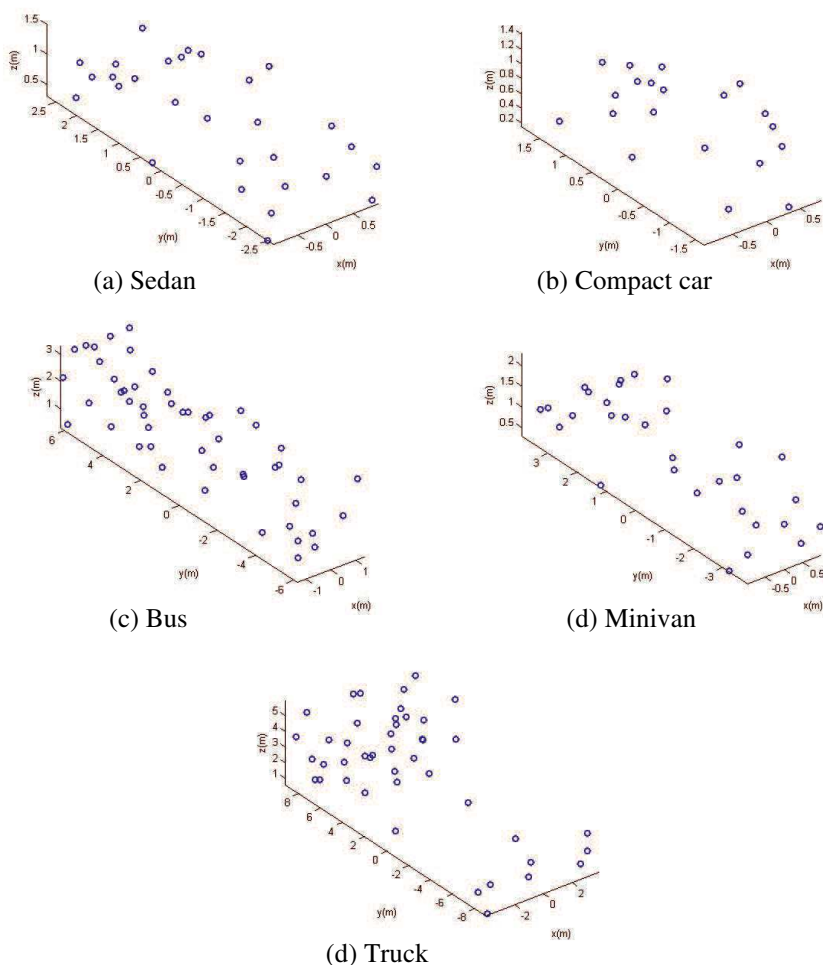(d) Minivan

(d) Truck

Figure 3. Automobiles used for simulation.

of range bins because of the narrow bandwidth $= 30\,\text{MHz}$ (Fig. 4).

The training database was constructed using RPs derived at angles sampled with an increment $\Delta\theta$ in a given azimuth aspect angle between $-\theta_R$ and θ_R, and the effects of various $\Delta\theta$s and θ_Rs were simulated. The test data were derived at a random angle between $-\theta_R$ and θ_R. Then the correct classification ratio P_c, which is the ratio between the number of correctly classified test vectors and that of the number of the total test vectors, was used as a performance measure. To simulate the
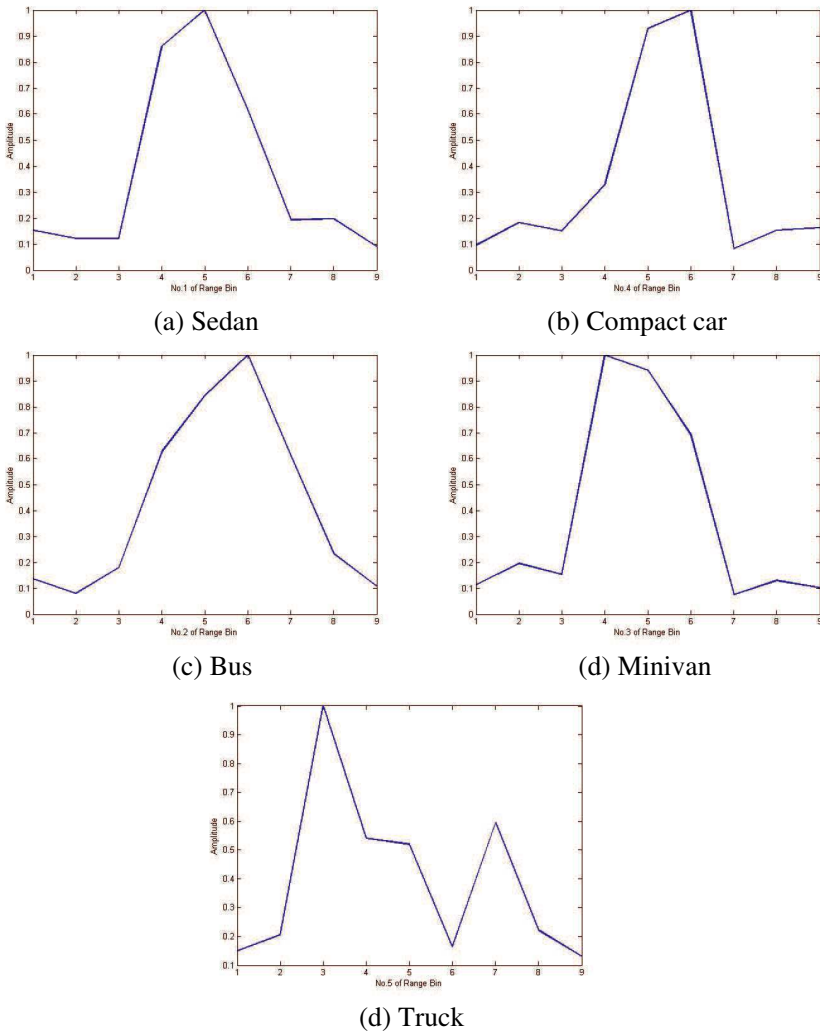

(a) Sedan   (b) Compact car

(c) Bus   (d) Minivan

(d) Truck

Figure 4. RPs of the automobiles in Fig. 3 ($B = 30\,\text{MHz}$).

effect of RP fluctuation caused by the clutter, $a \times \bar{p}(n)$ was subtracted from $\bar{p}(n)$ for each n, where a is a random number between $-h$ and h.

Using $a_m = 3$ for MMI and $n_m = 2$ for PI (see (13) $\sim$ (17)), various classification results obtained by using feature vectors CM only, CM + MMI, CM + PI and CM + MMI + PI were compared to demonstrate the efficiency of the proposed method. To further improve the classification result, a multi-aspect classification was conducted using (25) and the test RPs collected from each automobile moving for 1 sec at a random relative velocity between -11.11 and $11.11\,\mathrm{m/s}$ (-40 and $40\,\mathrm{km/h}$, respectively) and a random acceleration between -2 and $2\,\mathrm{m/s}^2$. The test RPs were down-sampled to 20 to save the computation time. To remove the effect of the randomness, each simulation was conducted 10 times and the average was used as a P_c. In selecting O for PCA, the number of the highest eigen vectors whose the sum was larger than 99% of the total sum was selected.

In the single-aspect classification, P_c derived by using CMs only with $\Delta\theta = 0.1°$, $\theta_R = 10°$ and $h = 0.1$ was not seriously affected by the P_m because of the narrow bandwidth (Fig. 5(a)); P_c ranged between 36.8 and 33.6%. Therefore, P_m was set to 5 in the following simulations to save the memory space. In the single-aspect classifications using $h = 0.1$, P_cs increased in proportion to SNR, and the classification result obtained by using a combination of CM + PI + MMI was considerably improved (Fig. 5(b)).

Compared with CM only, the result was improved with the amount of improvement (ΔP_c) $20.8\% \leq \Delta P_c \leq 27.2\%$. P_cs of CM + MMI was higher than CM + PI because MMI utilized relative the information between MMs and PI utilized the peak information only. Compared with the single-aspect classification (Fig. 6(a)), P_cs of multi-aspect classification derived by using SNR $= 10\,\mathrm{dB}$, $\Delta\theta = 0.1°$ and $h = 0.1$ for various θ_Rs improved considerably (Fig. 6(b)); P_cs of CM + MMI and CM + PI + MMI were approximately equal to 95%, those of

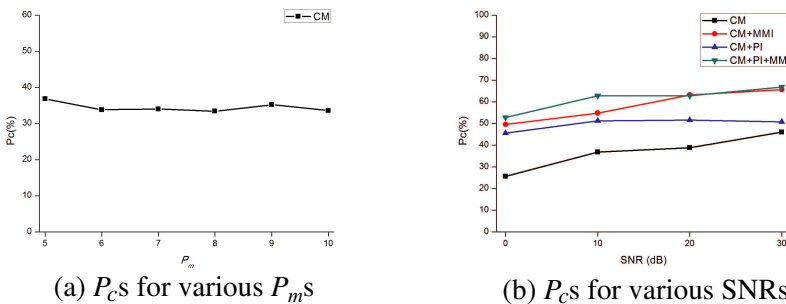(a) P_cs for various P_ms

(b) P_cs for various SNRs

Figure 5. P_cs for various P_ms and SNRs.

CM + PI and CM were approximately $75.0\% \leq P_c \leq 80.0\%$ and $65.0\% \leq P_c \leq 70.0\%$. P_cs of CM + PI + MMI were slightly higher than those of CM + MMI. Comparison of CM + PI and CM + MMI proves that MMI contains more information that helps to discriminate the targets than does CP.

Comparison of the results conducted by using SNR = 10 dB, $\theta = 10°$ and $h = 0.1$ for various $\Delta\theta$s shows a result similar to that in Fig. 6 (Fig. 7); CM + PI + MMI and CM + MMI yielded much higher results than CM + PI and CM did. As $\Delta\theta$ increased, P_cs decreased because of the reduction of the training data. However, the proposed method still provided P_cs higher than 95%.

The proposed method was much more robust to fluctuation (Fig. 8). As h becomes larger, the test RP can be more different from the train RP because of the increased fluctuation, and this yields discrepancy of high order CMs. Consequently, the classification result of CM and MMI decreased considerably in both single- and multiple-aspect classifications. However, the proposed method was unaffected by fluctuation because of the increased information provided by PI
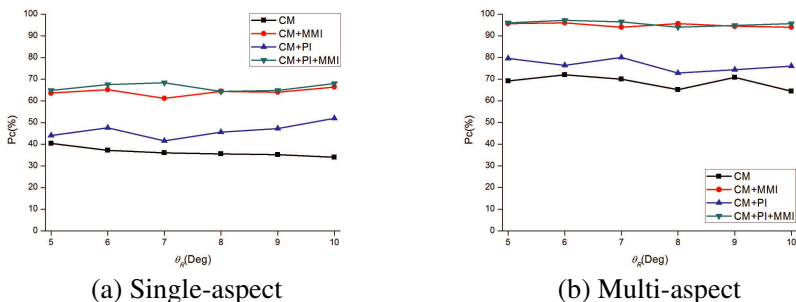

(a) Single-aspect   (b) Multi-aspect

Figure 6. Comparison of P_cs for various θ_Rs.

(a) Single-aspect   (b) Multi-aspect
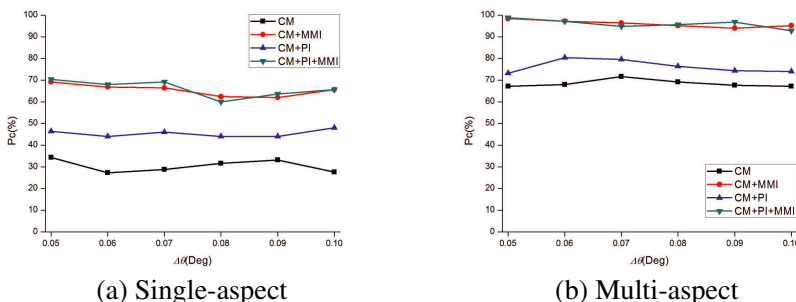
Figure 7. Comparison of P_cs for various θs.

(a) Single-aspect   (b) Multi-aspect
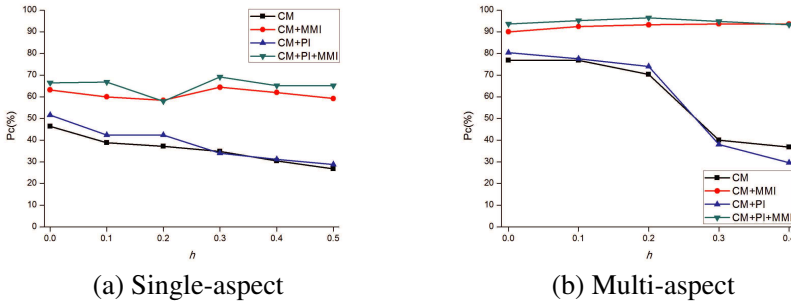
Figure 8. Comparison of P_cs for various hs; fluctuation of RP is proportional to h.

and MMI. Similar to the results in Figs. 6 and 7, the increase of P_cs by MMI was larger than that by PI.

4. CONCLUSION

CM of RPs has been proven a very efficient feature to classify targets using the radar, and this can be effectively applied to the recognition of automobiles. However, the major problem of CM is the fluctuation of higher order CMs caused by the fluctuation of RPs of an automobile influenced by its surroundings. In addition, the limited radar bandwidth further degrades the classification performance. To solve this problem, we proposed a combination of useful features that improve the classification result using low-resolution RPs of automobiles; in addition to CM, PI and MMI were combined to further improve P_cs. In simulations that applied scatters modeled by using the real-sized CAD data of five automobiles, the proposed method yielded high classification results that were insensitive to the range of aspect angle, the size of training database, and the fluctuation of RPs. Compared with CM only, a significant improvement of P_cs was achieved by the proposed method. At SNR = 10 and $h = 0.1$; P_cs higher than 95% was provided by CM + PI + MMI in multi-aspect classification. The improvement by MMI was much higher than that by PI because of the relatively rich information between MMs.

In this paper, we proposed two simple types of features to improve the classification of automobiles which yielded very impressive results. Because there can be other efficient features such as the histogram, combination of the proposed method and these other features may further improve the classification result. Moreover, because the NNC used in this paper is a very simple classifier, a more efficient classifier such as the neural network classifier may be used for greater

improvement of performance. Therefore, we are currently exploring new features and new classifiers that can significantly improve the classification result.

ACKNOWLEDGMENT

REFERENCES

1. Almeida, M., *Advances in Vehicular Networking Technologies*, InTech, 2011.
2. De Cos, M. E., Y. A. Lopez, and F. L. H. Andres, "On the influence of coupling AMC resonances for RCS reduction in the SHF band," *Progress In Electromagnetics Research*, Vol. 117, 103–119, 2011.
3. De Cos, M. E., Y. A. Lopez, and F. L. H. Andres, "A novel approach for RCS reduction using a combination of artificial magnetic conductors," *Progress In Electromagnetics Research*, Vol. 107, 147–159, 2010.
4. Costa, F., S. Genovesi, and A. Monorchio, "A frequency selective absorbing ground plane for low-RCS microstrip antenna arrays," *Progress In Electromagnetics Research*, Vol. 126, 317–332, 2012.
5. Park, H.-G., K. K. Park, H.-T. Kim, and K.-T. Kim, "Improvement of RCS prediction using modified angular division algorithm," *Progress In Electromagnetics Research*, Vol. 123, 105–121, 2012.
6. Park, H.-G., H.-T. Kim, and K.-T. Kim, "Beam tracing for fast RCS prediction of electrically large targets," *Progress In Electromagnetics Research M*, Vol. 20, 29–42, 2011.
7. Vaitilingom, L. and A. Khenchaf, "Radar cross sections of sea and ground clutter estimated by two scale model and small slope approximation in HF-VHF bands," *Progress In Electromagnetics Research B*, Vol. 29, 311–338, 2011.
8. Escot-Bocanegra, D., D. Poyatos-Martınez, I. Montiel-Sanchez, F. M. Saez de Adana, and I. Gonzalez-Diego, "Spherical indoor facility applied to bistatic radar cross section measurements," *Progress In Electromagnetics Research Letters*, Vol. 26, 181–187, 2011.

9. Shang, Y., S.-Q. Xiao, J.-L. Li, and B.-Z. Wang, "An electronically controllable method for radar cross section reduction for a microstrip antenna," *Progress In Electromagnetics Research*, Vol. 127, 15–30, 2012.

10. Machowski, W., G. S. Koutsogiannis, and S. Potter, "A novel approach to range profile estimation of a moving vehicle by road monitoring radar," *2007 IET International Conference on Radar Systems*, 1–5, 2007.

11. Yang, W., Y. Liu, G.-S. Xia, and X. Xu, "Statistical mid-level features for building-up area extraction from full polarimetric SAR imagery," *Progress In Electromagnetics Research*, Vol. 132, 233–254, 2012.

12. Ren, X.-Z., Y. F. Li, and R. Yang, "Four-dimensional SAR imaging scheme based on compressive sensing," *Progress In Electromagnetics Research B*, Vol. 39, 225–239, 2012.

13. Yan, S., Y. Li, T. Jin, Z.-M. Zhou, and D. X. An, "Improved motion compensation for wide-beam wide-swath airborne SAR," *Progress In Electromagnetics Research Letters*, Vol. 36, 1–7, 2013.

14. Yan, W., J.-D. Xu, G. Wei, L. Fu, and H.-B. He, "A fast 3D imaging technique for near-field circular SAR processing," *Progress In Electromagnetics Research*, Vol. 129, 271–285, 2012.

15. Quivira, F., J. A. Martinez-Lorenzo, and C. M. Rappaport, "Impact of the wave number estimation in underground focused SAR imaging," *Progress In Electromagnetics Research Letters*, Vol. 32, 29–38, 2012.

16. Fan, C., X.-T. Huang, T. Jin, J.-G. Yang, and D. X. An, "Novel pre-processing techniques for coherence improving in along-track dual-channel low frequency SAR," *Progress In Electromagnetics Research*, Vol. 128, 171–193, 2012.

17. Liu, Y., Y.-K. Deng, R. Wang, and X. Jia, "Bistatic FMCW SAR raw signal simulator for extended scenes," *Progress In Electromagnetics Research*, Vol. 128, 479–502, 2012.

18. Park, S.-H., J.-I. Park, and K.-T. Kim, "Bistatic FMCW SAR raw signal simulator for extended scenes," *Progress In Electromagnetics Research*, Vol. 128, 479–502, 2012.

19. Liu, J., X. Li, S. Xu, and Z. Zhuang, "ISAR imaging of non-uniform rotation targets with limited pulses via compressed sensing," *Progress In Electromagnetics Research B*, Vol. 41, 285–305, 2012.

20. Park, J.-H., H. Lim, and N.-H. Myung, "Modified Hilbert-Huang transform and its application to measured micro Doppler

signatures from realistic jet engine models," *Progress In Electromagnetics Research*, Vol. 126, 255–268, 2012.

21. Han, S.-K., H.-T. Kim, S.-H. Park, and K.-T. Kim, "Efficient radar target recognition using a combination of range profile and time-frequency analysis," *Progress In Electromagnetics Research*, Vol. 108, 131–140, 2010.

22. Kim, K.-T. and H.-R. Jeong, "Identification of multi-aspect radar signals based on the feature space trajectory concept," *IEEE Transations on Antennas and Propagation*, Vol. 53, No. 11, 3811–3821, Nov. 2005.

23. Park, S.-H., J.-H. Lee, and K.-T. Kim, "Performance analysis of the scenario-based construction method for real target ISAR recognition," *Progress In Electromagnetics Research*, Vol. 128, 137–151, 2012.

24. Park, S.-H., M.-G. Joo, and K.-T. Kim, "Construction of ISAR training database for automatic target recognition," *Journal of Electromagnetic Waves and Applications*, Vol. 25, Nos. 11–12, 1493–1503, 2011.

25. Park, S.-H., "Automatic recognition of targets in formation using range profiles," *Journal of Electromagnetic Waves and Applications*, Vol. 26, Nos. 14–15, 2059–2069, Oct. 2012.

26. Li, Q., E. J. Rothwell, K. M. Chen, and D. P. Nyquist, "Radar target discrimination schemes using time-domain and frequency-domain methods for reduced data storage," *IEEE Transaction on Antennas and Propagation*, Vol. 45, 995–1000, Jun. 1997.

27. Zyweck, A. and R. E. Bogner, "Radar target classfication of commercial aircraft," *IEEE Transactions on Aerospace Electronic Systems*, Vol. 32, 598–606, Apr. 1996.

28. Luo, S. and S. Li, "Automatic target recognition of radar HRRP based on high order central moments features," *Journal of Electronics (China)*, Vol. 26, No. 2, 184–190, Mar. 2009.

29. Cumming, I. G. and F. H. Wong, *Digital Processing of Synthetic Aperture Radar*, Artech House, 2005.

30. Sezan, M. L., "A peak detection algorithm and its application to histogram-based image data reduction," *Computer Vision, Graphics, and Image Processing*, Vol. 49, No. 1, 36–51, Jan. 1990.

31. Kim, K. T., D. K. Seo, and H. T. Kim, "Efficient radar target recognition using the MUSIC algorithm and invariant features," *IEEE Transaction on Antennas and Propagation*, Vol. 50, No. 3, 325–337, Mar. 2002.